SEMARAK ILMU PUBLISHING

Journal of Advanced Research in Fluid Mechanics and Thermal Sciences

Journal homepage:
https://semarakilmu.com.my/journals/index.php/fluid_mechanics_thermal_sciences/index
ISSN: 2289-7879

Applications of Computational Fluid Dynamics in the E-Cigarettes Industry

Lingquan Wang[1,2,*], Ge Nie[1], Liwei Xiao[1], Guanyun Zhao[1], Yueyong Chen[1], Chunhua Wei[1]

[1] Innovation Research Institute, Shenzhen Woody Vapes Technology Co., Ltd., Shenzhen, 518000, China
[2] School of Aeronautics and Astronautics, Chongqing University, Chongqing, 400000, China

ARTICLE INFO

Article history:
Received 22 February 2022
Received in revised form 3 May 2022
Accepted 8 May 2022
Available online 9 June 2022

Keywords:
E-cigarette; standard k-ε turbulent model; broadband noise source model; discrete phase model (DPM)

ABSTRACT

An advanced pod E-cigarette, launched by Shenzhen Woody Vapes Technology Co., Ltd., was researched and analysed in this paper with the help of computational fluid dynamics (CFD) simulation. The standard k-ε turbulent model was introduced to simulate the flow of air, the Broadband Noise Source model adapted to measure the noise and the Discrete Phase Model (DPM) used to calculate the trajectories of the aerosols. The pressure, velocity and noise fields, the trajectories of the aerosols, obtained by Reynolds-Averaged Navier-Stokes (RANS) simulation, were analysed to optimize the structure design of this pod system. Several related experiments were performed and significant improvement was also confirmed.

1. Introduction

The use and awareness of electronic cigarette (e-cigarette), which is known as representing an alternative nicotine delivery system to conventional combustible cigarettes, has increased rapidly in the past years [1-3]. The working principle of e-cigarette is to vaporize a solution containing nicotine to produce aerosol as a result of the mixture of cold air and hot vapor. As reported by Williams and Talbot [4], to increase the release of nicotine, these nicotine delivery systems usually improved significantly stronger airflow and higher pressure drop to produce aerosol. However, enhanced airflow will bring noise problems. Thus, an urgent problem confronting us is how to minimize noise under the premise of stronger airflow. And beyond that the emission of e-cigarettes is aerosol containing nicotine, water and glycerol, propylene glycol and flavors, etc. [5]. Due to the miniaturization of e-cigarette and the short residence time of aerosol in the airway, it is difficult to study the movement of aerosols by experimental methods. In recent years, with the rapid development of simulation technology, CFD has been applied to the study on the aerosol deposition in respiratory tract [6-15]. However, there are few related studies on aerosol motion and flow noise in electronic cigarette airway by CFD.

In order to study the characteristics of aerosol motion in the e-cigarette, it is necessary to establish a suitable mathematical model. Firstly, the aerosol produced by e-cigarette is a mixture of

* *Corresponding author.*
E-mail address: milas@voopoo.com

https://doi.org/10.37934/arfmts.96.1.7081

air and small droplets actually [5]. A number of studies have shown that the total particulate matter (TPM) of pod E-cigarette per puff is between 5mg and 15mg (about 0.004ml to 0.02ml) under pumping capacity at 55ml [16-18]. In other words, the volume concentration of the droplet is less than 0.1%. Thus, the flow of aerosol can be approximated as the flow of air in the e-cigarette without considering the motion of droplets [4]. In fact, the flow rate of pod E-cigarette was less than 30 mL/s according to vapers' mean puff duration and 17.5ml/s or 18.3ml/s is often used in actual experimental tests [4,17,20]. At the flow rate of 18.3ml/s, the flow velocity of aerosol in the E-cigarette airway is less than 30m/s, due to minimum hole size shall not be less than 0.5mm. Thus, the flow Mach number in the airway will not exceed 0.1, the aerosol flow in the e-cigarette can be regarded as incompressible air flow without considering the motion of droplets. In this article, the incompressible NS equations and the Broadband Noise model was adapted to describe the airflow and noise assessment inside the e-cigarette, which can be solved by the finite volume method [7,9,22,23]. In addition, when the aerosols contact the wall of the airway, some droplets will be captured by the wall, which will cause the formation of condensate liquid. To reduce the generation of condensate liquid, the droplets motion should be researched. The spherical droplets move with the air in the airway and its particle size satisfies the normal distribution. To obtain the droplets motion information, a discrete phase model was introduced to simulate the motion of droplets by getting these trajectories.

In this paper, we report an optimization method to research the aerosol motion inside the e-cigarette. The method, based on the CFD simulation, contained the model to calculate the suction resistance and airflow noise and the model to simulate the trajectories of the droplets. The accuracy of the method was also verified by the related experimental method. Then this method was applied to optimize the structure design of our ZOOVOO products.

2. Methodology

Firstly, as mentioned, the flow characteristics in the airway can be obtained by approximately continuous air flow. Secondly, as known, noise have no obvious frequency domain, and the sound energy is continuously distributed in a wide frequency range, which involves the problem of broadband noise. To model acoustic field in the e-cigarette, the broadband noise model is used, the turbulence parameters are obtained by the Reynolds time average equation, and then the acoustic power of the surface element or volume element is calculated by the semi empirical correction model [13,14,22-24]. In addition, to model the movement of aerosols in the e-cigarette, the Eulerian-Lagrangian approach is applied, known as the Discrete Phase Model (DPM) [15-17]. In CFD-DPM simulations, the fluid phase is modeled as a continuum while droplets are treated as a discrete phase [11,12,15]. In the DPM, the interaction between droplets and continuous phase can be unidirectional, which means that the fluid can affect the momentum and energy of droplets, but the movement of droplets will not affect the flow field of the continuous phase [26,27]. To account for particle-particle collisions, the DPM approach can be extended using the Discrete Element Method (DEM). To take the ZOOVOO product of Shenzhen Woody Technology Co., Ltd as an example, we apply these methods to help optimize the design of e-cigarettes.

2.1 Continuous Phase Modelling

A large number of test results show that the airflow in the e-cigarette can be treated as in-compressible flow [4,17,18,20,25]. Thus, the governing equations of airway fluid flow in the e-cigarette are given as [28]

$$\frac{\partial u_i}{\partial x_i} = 0 \tag{1}$$

$$\frac{\partial u_i}{\partial t} + \frac{\partial}{\partial x_j}\left(u_i u_j\right) = -\frac{1}{\rho}\frac{\partial p}{\partial x_i} + \frac{\partial u_i}{\partial x_j}\left[\vartheta\left(\frac{\partial u_i}{\partial x_i} + \frac{\partial u_i}{\partial x_j}\right) - \frac{\partial}{\partial x_i}\left(u_i^{'} u_j^{'}\right)\right] + g_i \tag{2}$$

Where ρrepresents the fluid density and ϑ its kinematic viscosity, u_i stands for the i_{th} time-averaged component of the fluid velocity, p the static pressure, t the time, x_i the i_{th} coordinate, δ_{ij} is the Kronecker delta, g_i the gravity term and $u_i^{'} u_j^{'}$, known as Reynolds-stress tensor, can be determined by the turbulence model. The general transport equations for the turbulence kinetic energy k and the turbulence dissipation rate ε of the standard $k - \varepsilon$ turbulent model, can be described as

$$\frac{\partial \rho k}{\partial t} + \frac{\partial}{\partial x_i}(\rho k u_i) = \frac{\partial}{\partial x_j}\left[\left(\mu + \frac{\mu_T}{\sigma_k}\right)\frac{\partial k}{\partial x_j}\right] + \mu_T\left(\frac{\partial u_i}{\partial x_k} + \frac{\partial u_k}{\partial x_i}\right)\frac{\partial u_i}{\partial x_k} - \rho\varepsilon \tag{3}$$

$$\frac{\partial \rho \varepsilon}{\partial t} + \frac{\partial}{\partial x_i}(\rho \varepsilon u_i) = \frac{\partial}{\partial x_j}\left[\left(\mu + \frac{\mu_T}{\sigma_\varepsilon}\right)\frac{\partial \varepsilon}{\partial x_j}\right] + C_{1\varepsilon}\frac{\varepsilon \mu_T}{k}\left(\frac{\partial u_i}{\partial x_k} + \frac{\partial u_k}{\partial x_i}\right)\frac{\partial u_i}{\partial x_k} - C_{2\varepsilon}\rho\frac{\varepsilon^2}{k} \tag{4}$$

where μ is the dynamic viscosity $C_{1\varepsilon}$=1.44 and$C_{2\varepsilon}$=1.92 are model constants, σ_k=1.0 andσ_ε=1.3 are the turbulent Prandtl numbers for k and ε, respectively.

2.2 Acoustic Field Modelling

Far-field sound, generated by turbulent boundary layer flow can be solved by the Broadband Noise Source Model. The acoustic pressure p' can be written as [29]

$$p'(\vec{x}, t) = \frac{1}{4\pi a_0}\int \frac{(x_i - y_i)n_i}{r^2}\frac{\partial p\left(\vec{x}, t - \frac{a_0}{r}\right)}{\partial t} dS(\vec{y}) \tag{5}$$

where a_0 is the far-field sound speed, $t - \frac{a_0}{r}$ the emission time, n_i the wall-normal direction and S represents the integration surface. Thus, the sound intensity in the far field can then be approximated by

$$\overline{p'^2}(\vec{x}, t) = \frac{1}{(4\pi a_0)^2}\int \frac{cos^2\theta}{r^2}\frac{\partial p\left(\vec{x}, t - \frac{a_0}{r}\right)^2}{\partial t} A_c(\vec{y}) dS(\vec{y}) \tag{6}$$

where A_c is the correlation area and $\theta$is the angle between $(x_i - y_i)$ and the wall-normal direction n_i. The measure of the local contribution to acoustic power per unit surface, known as Surface Acoustic Power (SAP), can be computed from

$$SAP = \frac{1}{\rho a_0}\left[\int_0^{2\pi}\int_0^{\pi} \overline{p'^2}\, r^2 sin\theta d\theta d\gamma\right] = \int I(\vec{y}) dS(\vec{y}) = \int \frac{A_c(\vec{y})}{12\pi\rho a_0^3}\overline{\left(\frac{\partial p}{\partial t}\right)^2}\, dS(\vec{y}) \tag{7}$$

where $I(\vec{y})$ is the directional acoustic intensity per unit surface. The SAP can be also reported in dimensional units(W/m^2) and in dB

$$SAP(\text{dB}) = 10\log\frac{SAP}{p_{ref}} \tag{8}$$

2.3 Discrete Phase Modelling

The droplets can be solved as a discrete phase, and the trajectories of the droplets can be computed by the Second Newtonian Law. Through integrating the force balance written in a Lagrangian reference frame, the governing equations of the droplets can be shown as [30]

$$\frac{d\overrightarrow{u_d}}{dt} = F_D + \vec{g}\frac{\rho_d - \rho}{\rho_d} + \vec{F} \tag{9}$$

where $\vec{u}$ is the fluid velocity, $\overrightarrow{u_d}$ the droplet velocity, ρ_d the droplet density, $\vec{F}$ denotes an additional acceleration term and $F_D(\vec{u} - \overrightarrow{u_d})$ is the drag force per unit mass, given by

$$F_D = \pi d_p^2 C_D(\vec{u} - \overrightarrow{u_d})|\vec{u} - \overrightarrow{u_d}|/8 \tag{10}$$

where d_p is the droplets diameter and the drag coefficient C_D for spherical droplets can be defined as

$$C_D = \frac{a_1}{Re_d} + \frac{a_2}{Re_d^2} + a_3 \tag{11}$$

where a_1, a_2, and $a_3$are coefficients determined by the relative Reynolds number Re_d, which can be calculated as

$$Re_d = \frac{\rho d_p|\vec{u} - \overrightarrow{u_d}|}{\mu} \tag{12}$$

2.4 Boundary Conditions and Numerical Schemes

In order to match the actual situation, pressure-inlet and mass-flow-outlet boundary condition were used for the simulations. The no-slip boundary condition was adapted in the walls. The droplet size distribution was positive and the injection mass flow of droplets was fixed. For the pressure-inlet inlet and mass-flow-outlet an “escape” condition is prescribed and near the solid boundaries a “trap” condition is prescribed.

In this paper, the CFD software Fluent 19.2 is used for modelling the fluid flow, the acoustic field analysis and the movement of droplets. The transport equations for the fluid flow were solved using the segregated Coupled algorithm. The gradients were discretized using the Least Square Cell Based, Pressure and Momentum using a second order upwind scheme and turbulent energy and turbulent dissipation using a first order upwind scheme, respectively. Particle tracking was carried out by an implicit trapezoidal rule and a particle time step was set of 5E10^{-5}s. A convergence tolerance of 10^{-5}s was used in all simulations.

The strategy during the solution procedure can be summarized in the following steps

i. The flow field without droplets is first calculated with steady state to convergence.
ii. The Broadband Noise Source Model is introduced to simulate the acoustic field.
iii. Close the Broadband Noise Source Model and the DPM is introduced to calculate the droplets trajectories.

3. Results

3.1 Main Characteristics of the Flow Field

The simulation is carried out in an e-cigarette as shown in Figure 1. The flow field without droplets is first calculated with steady state to convergence with the following conditions as shown in Table 1. To check of grid independence, a preliminary test about grid independence of the computational domain showed that it is unnecessary to increase the number of the cells beyond that it is unnecessary to increase the number of the cells beyond 1188690 as shown in Figure 2. Similar to the method in a study by Liu *et al.,* [21], Table 2 presents the comparison between the numerical results and the experimental data. According to comparison, one can see that all the four turbulence models may produce the acceptable prediction.

Figure 3 shows the air velocity profiles in vertical middle plane and Figure 4 shows the streamlines in the airway of the E-cigarette. From Figure 3 and Figure 4, the cross-sectional area of the flow passage changes suddenly, a larger velocity field will be generated, in which the maximum velocity occurs in the narrow inlet passage at the entrance. The air velocity profile has a great influence on the pressure drop and the pressure profiles are present in the Figure 5. The pressure drop at the inlet and outlet of the airway was 505Pa. To verify the accuracy of the results from the study by Williams and Talbot [4], the pressure drops under different test conditions were simulated and the experimental results were displayed in Figure 6. The errors between the present and average experimental results were shown in Table 3. As shown, the simulation results were in good agreement with the experimental results.

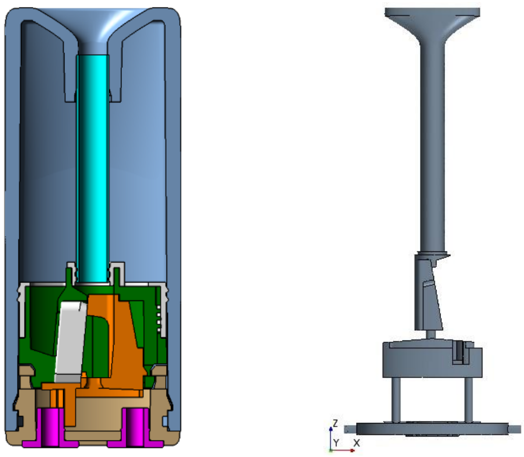

(a) (b)

Fig. 1. Schematic drawing of an e-cigarette (a) Structure diagram of atomization chamber and (b) the airway in the e-cigarette

Table 1
The physical parameters and simulation conditions

Parameter	Value
Inlet pressure (Pa)	101325
Outlet volume flow rate (ml/s)	18.3
Density of air (kg/m^3)	1.225

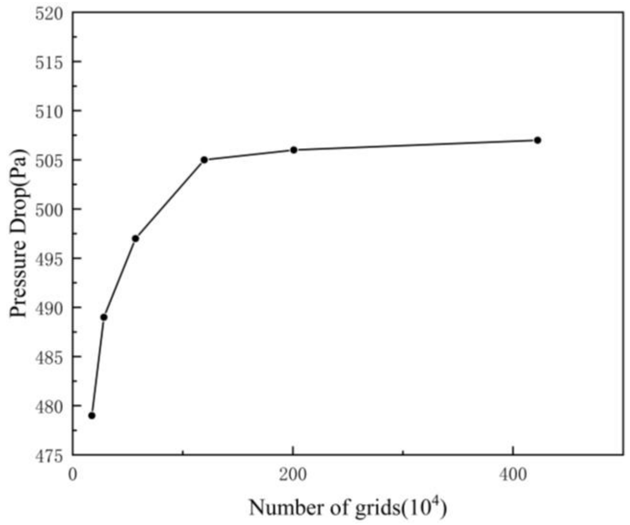

Fig. 2. The results of grid independence verification

Table 2
Performance of turbulence models in predicting experimental results

Turbulence models	Predicting results (Pa)	Experiment results (Pa)	Error (%)
Standard $k-\varepsilon$	505	521	3.1
Realizable $k-\varepsilon$	511	521	1.9
Standard $k-\omega$	496	521	4.8
SST $k-\omega$	501	521	3.8

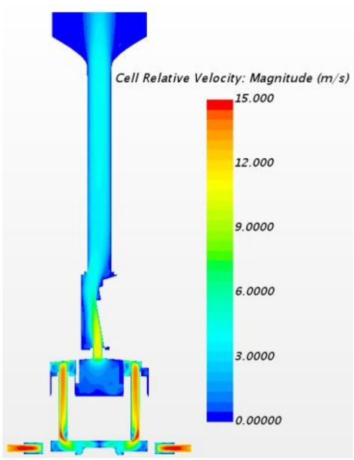

Fig. 3. Air velocity profiles in vertical middle plane

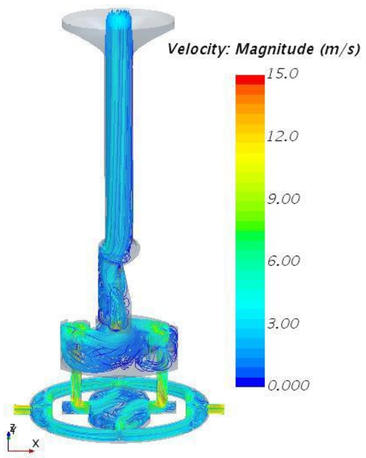

Fig. 4. Streamlines in the airway of the E-cigarette

Fig. 5. Pressure profiles in the airway of the E-cigarette

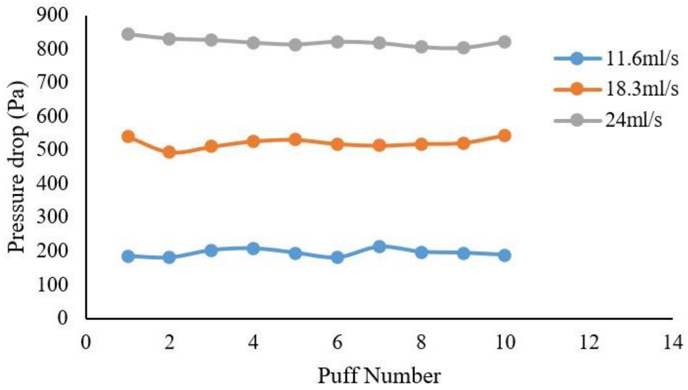

Fig. 6. The pressure drops under different test conditions

Table 3
The physical parameters and simulation conditions

Volume flow rate (ml/s)	Present results (Pa)	Experiment results (Pa)	Error (%)
11.6	204	194	4.7
18.3	505	521	3.1
24	786	820	4.1

In fact, the product's resistance requirement is 700Pa. To match this resistance, the inlet diameter is adjusted from 1mm to 0.6mm and the pressure drops are shown in Table 4. The pressure drop will increase to 694Pa, when the inlet diameter is designed to be 0.8mm.

Table 4
Pressure drops in the airway with different inlet diameters

Inlet diameter (mm)	Pressure drops (Pa)
1	505
0.8	694
0.6	1399

3.2 Acoustic Fields of the E-cigarette

Open the Broadband Noise Source Model, the acoustic fields can be simulated present as Figure 7. The maximum speed occurs where the section area is smallest. Through the distribution cloud of sound field intensity, it can be seen that there will be a larger sound field intensity at the abrupt change of the passage, especially near the bend of the entrance. Therefore, it is necessary to smooth the bend to avoid the sudden change of physical field and reduce the intensity of turbulent flow field, so as to reduce the airway noise. As shown in Figure 8, after optimization, the sound field intensity and the noise of the airway are reduced and the maximum acoustic power is reduced to 100.6dB.

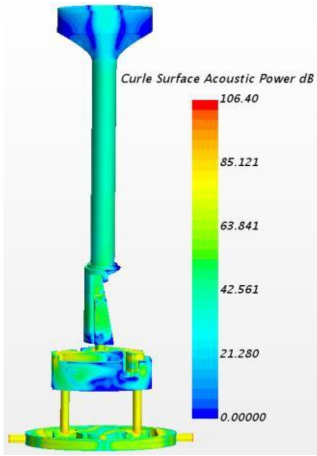

Fig. 7. Acoustic fields in the airway

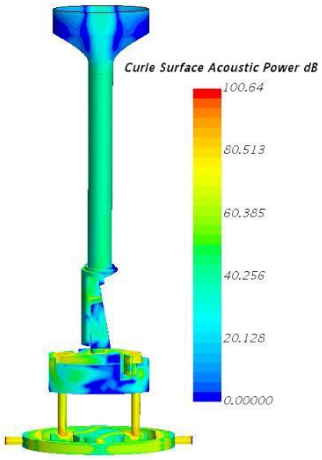

Fig. 8. Optimized acoustic fields in the airway

3.3 The Droplets Trajectories in the Airway

CFD results obtained with the droplet transport model applied to airway are presented. The additional physical parameters are displayed in Table 5. As shown in Figure 9 and Figure 10, trajectory of the discrete phase movement and cloud diagram of droplet attachment are presented. It can be seen that air velocity has great influence on droplets velocity and size distribution. The movement of the droplets is consistent with the flow of air and as the flow develops, larger droplets gradually move closer to the wall. As presented in Figure 9, there are fewer particles in the middle area of the pipe. The reason is that the large air flow rate of the injecting surface and the offset of the air flow velocity on the cross-section as displayed in Figure 11 result in the separation of particle flow.
In order to verify the accuracy of the results, The adhesion rate of the wall is calculated by simulation and experiment results, respectively. The adhesion rate of experimental test φ_e and the adhesion rate of simulation φ_c can be calculated as:

Table 5
The physical parameters of droplets

Parameter	Value
Density of droplet(kg/m^3)	1130
Injecting flow rate(mg/s)	3.3
Density of vapor (kg/m^3)	3.1
Mean particle size(μm)	0.745

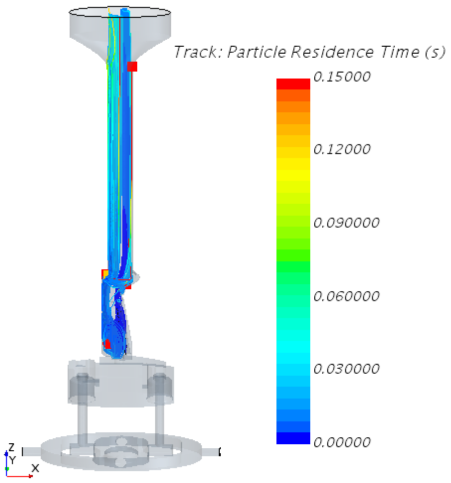

Fig. 9. The trajectories of the discrete droplets in the airway

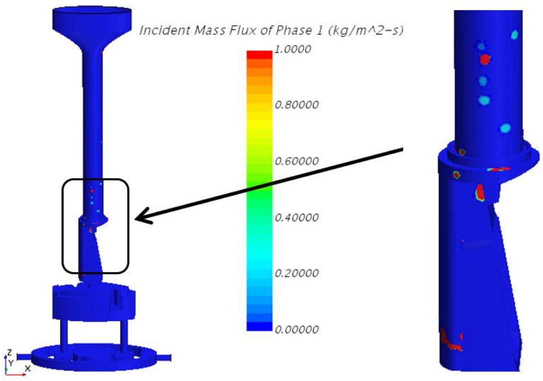

Fig. 10. The cloud diagram of droplet attachment in the airway

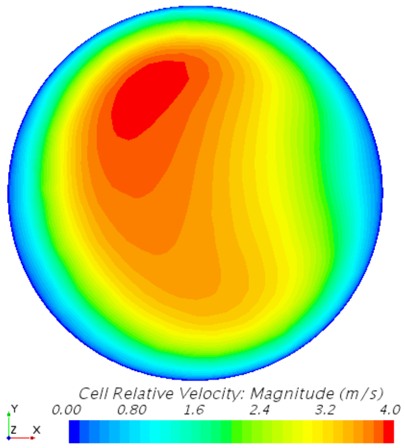

Fig. 11. Air velocity profiles at cross-section of Z=20mm

$$\varphi_e = 1 - \frac{m_1 - m_2}{m_{oil}} \tag{13}$$

$$\varphi_c = 1 - \frac{Q_{in} - Q_{out}}{Q_{in}} \tag{14}$$

where m_1 represents the initial mass of atomizing bomb, m_2 the mass of atomizing bomb after suction, m_{oil} the mass of oil, Q_{in} the injection particle flow, and Q_{out} the particle flow of the outlet. The main experimental steps are described as following

i. Inject 2ml oil into the atomizing bomb, and record the weight of the smoke oil m_{oil}
ii. Measuring the initial mass of atomizing bomb m_1
iii. According to the suction standard in the literature until the oil is exhausted, then measuring the mass of atomizing bomb m_2 [4]
iv. Calculate the adhesion rate.

Figure 12 show a comparison of the simulated adhesion rate against 100 experiments for the airway. As can be seen, As can be seen, simulate adhesion rate are now mainly within 5% of the measured values and it is feasible to simulate the motion of droplets in the airway with the DPM model. In addition, most of the experimental values are higher than simulated results, because little oil in the atomizing bomb could not be consumed completely in the experimental tests.

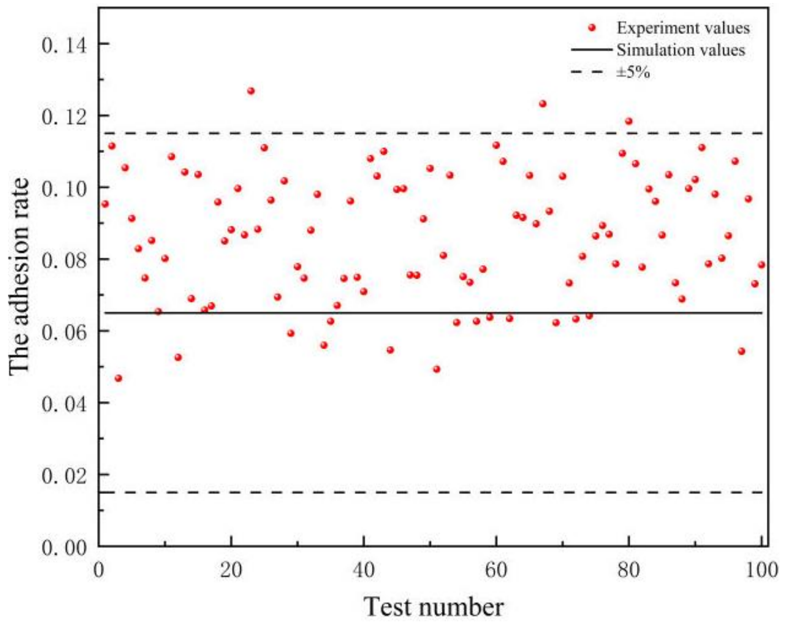

Fig. 12. Comparison of the simulated adhesion rate against 100 experiments

To reduce wall adhesion, the cases with different diameters of the cross-section below the injecting surface and pressure drop, as shown in Table 6, are performed and the adhesion rates of different cases are calculated. As seen, with the diameter of the cross-section below the injecting surface decreasing and the volume flow rate increasing, the velocity of the droplet increases and the adhesion rate will increase. Higher velocity also leads to larger pressure drop. Thus, a larger pressure drop helps reduce the adhesion rate.

Table 6
The adhesion rates of different cases

Case number	Volume flow rate (ml/s)	Area of the cross-section (mm^2)	The adhesion rate
1	18.3	2.183	6.7%
2	11.6	2.183	4.2%
3	24.0	2.183	9%
4	18.3	3.417	8.4%
5	18.3	1.201	6.1%

4. Conclusions

An optimization method has been successfully applied to help the structure design of E-cigarettes. The method can not only help to evaluate the suction resistance and sound noise of the airway inside the E-cigarette, but also calculate the location of droplets accumulation and the effectiveness of this method has been proved by comparing with the experimental results. Several findings of simulation work can be summarized as following

i. The flow characteristics of aerosols in the E-cigarette airway can be approximately calculated by incompressible air and the pressure drop can be increased by reducing the inlet diameter of the airway.
ii. Smoothing the suddenly changing section and reducing flow vortex can effectively weaken the intensity of the sound field.
iii. It is appropriate to simulate the motion of aerosols in the airway with the DPM model. In addition, reducing the airflow cross-section below the injecting surface can increase the air velocity and pressure drop, and stronger airflow and higher pressure drop contribute to reducing wall adhesion.

Acknowledgement
This work was financially supported by Innovation Research Institute of Shenzhen Woody Vapes Technology Co., Ltd.

References
[1] Etter, Jean-François. "Electronic cigarettes: a survey of users." *BMC Public Health* 10, no. 1 (2010): 1-7. https://doi.org/10.1186/1471-2458-10-231
[2] Adkison, Sarah E., Richard J. O'Connor, Maansi Bansal-Travers, Andrew Hyland, Ron Borland, Hua-Hie Yong, K. Michael Cummings et al. "Electronic nicotine delivery systems: international tobacco control four-country survey." *American Journal of Preventive Medicine* 44, no. 3 (2013): 207-215. https://doi.org/10.1016/j.amepre.2012.10.018
[3] Gallus, Silvano, Alessandra Lugo, Roberta Pacifici, Simona Pichini, Paolo Colombo, Silvio Garattini, and Carlo La Vecchia. "E-cigarette awareness, use, and harm perceptions in Italy: a national representative survey." *Nicotine & Tobacco Research* 16, no. 12 (2014): 1541-1548. https://doi.org/10.1093/ntr/ntu124
[4] Williams, Monique, and Prue Talbot. "Variability among electronic cigarettes in the pressure drop, airflow rate, and aerosol production." *Nicotine & Tobacco Research* 13, no. 12 (2011): 1276-1283. https://doi.org/10.1093/ntr/ntr164
[5] Fuoco, Fernanda Carmen, Giorgio Buonanno, Luca Stabile, and Paolo Vigo. "Influential parameters on particle concentration and size distribution in the mainstream of e-cigarettes." *Environmental Pollution* 184 (2014): 523-529. https://doi.org/10.1016/j.envpol.2013.10.010
[6] Soni, Sanjay Kumar, Amarjit Singh, Manmohan Sandhu, Aashish Goel, and Ram Kumar Sharma. "Numerical simulation to investigate the effect of obstacle on detonation wave propagation in a pulse detonation engine combustor." *International Journal of Emerging Technology and Advanced Engineering* 3, no. 3 (2013): 458-464.
[7] Abd Rahman, Muhammad Faqhrurrazi, Nor Zelawati Asmuin, Ishkrizat Taib, Mohamad Nur Hidayat Mat, and Riyadhthusollehan Khairulfuaad. "Influence of Actuator Nozzle Angle on the Flow Characteristics in Pressurized-Metered Dose Inhaler Using CFD." *CFD Letters* 12, no. 6 (2020): 67-79. https://doi.org/10.37934/cfdl.12.6.6779
[8] Sharma, Pavan K., B. Gera, and R. K. Singh. "Application of RANS and LES Based CFD to Predict the Short and Long Term Distribution and Mixing of Hydrogen in a Large Enclosure." *CFD Letters* 3, no. 1 (2011): 18-31.
[9] Zainal, S., C. Tan, C. J. Sian, and T. J. Siang. "ANSYS simulation for Ag/HEG hybrid nanofluid in turbulent circular pipe." *Journal of Advanced Research in Applied Mechanics* 23, no. 1 (2016): 20-35.
[10] Elfaghi, Abdulhafid M. A., Alhadi A. Abosbaia, Munir F. A. Alkbir, and Abdoulhdi A. B. Omran. "CFD Simulation of Forced Convection Heat Transfer Enhancement in Pipe Using Al2O3/Water Nanofluid." *Journal of Advanced Research in Numerical Heat Transfer* 8, no. 1 (2022): 44-49.

[11] Doroshenko, Yaroslav, Julia Doroshenko, Vasyl Zapukhliak, Lyubomyr Poberezhny, and Pavlo Maruschak. "Modeling computational fluid dynamics of multiphase flows in elbow and T-junction of the main gas pipeline." *Transport* 34, no. 1 (2019): 19-29. https://doi.org/10.3846/transport.2019.7441
[12] Solihin Musa, Nor Azwadi Che Sidik, Siti Nurul Akmal Yusof, and Erdiwansyah Erdiwansyah. "Analysis of Internal Flow in Bag Filter by Different Inlet Angle." *Journal of Advanced Research in Numerical Heat Transfer* 3, no. 1 (2020): 12-24.
[13] Tian, Geng, and P. Longest. "Development of a CFD boundary condition to model transient vapor absorption in the respiratory airways." *Journal of Biomechanical Engineering* 132, no. 5 (2010). https://doi.org/10.1115/1.4001045
[14] Zhang, Zhe, Clement Kleinstreuer, and Yu Feng. "Vapor deposition during cigarette smoke inhalation in a subject-specific human airway model." *Journal of Aerosol Science* 53 (2012): 40-60. https://doi.org/10.1016/j.jaerosci.2012.05.008
[15] Chen, Xiaole, Wenqi Zhong, Baobin Sun, Baosheng Jin, and Xianguang Zhou. "Study on gas/solid flow in an obstructed pulmonary airway with transient flow based on CFD-DPM approach." *Powder Technology* 217 (2012): 252-260. https://doi.org/10.1016/j.powtec.2011.10.034
[16] Cheng, Tianrong. "Chemical evaluation of electronic cigarettes." *Tobacco Control* 23, no. suppl 2 (2014): ii11-ii17. https://doi.org/10.1136/tobaccocontrol-2013-051482
[17] Jin, J., Y. Zhang, Y. Zhang, S. Zheng, and W. Gu. "Effects of smoking regimen and parameter on e-cigarette TPM delivery of its aerosol." *Tobacco Science & Technology* 49, no. 6 (2016): 65-70. https://doi.org/10.16135/j.issn1002-0861.20160610
[18] Hasan, Farhana, Lavrent Khachatryan, and Slawo Lomnicki. "Comparative studies of environmentally persistent free radicals on total particulate matter collected from electronic and tobacco cigarettes." *Environmental Science & Technology* 54, no. 9 (2020): 5710-5718. https://doi.org/10.1021/acs.est.0c00351
[19] Cunningham, Anthony, Sandra Slayford, Carl Vas, Jodie Gee, Sandra Costigan, and Krishna Prasad. "Development, validation and application of a device to measure e-cigarette users' puffing topography." *Scientific Reports* 6, no. 1 (2016): 1-7. https://doi.org/10.1038/srep35071
[20] Kuga, Kazuki, Kazuhide Ito, Wenhao Chen, Ping Wang, and Kazukiyo Kumagai. "A numerical investigation of the potential effects of e‐cigarette smoking on local tissue dosimetry and the deterioration of indoor air quality." *Indoor Air* 30, no. 5 (2020): 1018-1038. https://doi.org/10.1111/ina.12666
[21] Liu, Xingwei, Zhongliang Liu, and Yanxia Li. "Investigation on separation efficiency in supersonic separator with gas-droplet flow based on DPM approach." *Separation Science and Technology* 49, no. 17 (2014): 2603-2612. https://doi.org/10.1080/01496395.2014.938755
[22] Mat, Mohamad Nur Hidayat, Nor Zelawati Asmuin, Nor Halim Hasan, Hanis Zakaria, Muhammad Faqhrurrazi Abd Rahman, Riyadhthusollehan Khairulfuaad, and Balasem Abdulameer Jabbar. "Optimizing dry ice blasting nozzle divergent length using CFD for noise reduction." *CFD Letters* 11, no. 6 (2019): 18-26.
[23] Sravani, Vemuri, S. Srinivas Prasad, M. Ravi Teja, and K. Ramanaiah. "Acoustic analysis of ship propeller using CFD." *International Journal of Ambient Energy* (2020): 1-5. https://doi.org/10.1080/01430750.2020.1848916
[24] Stanko, Tanya S., Derek B. Ingham, Michael Fairweather, and Mohamed Pourkashanian. "Computational fluid dynamic prediction of noise from a cold turbulent propane jet." In *Turbo Expo: Power for Land, Sea, and Air*, vol. 43130, pp. 645-652. 2008. https://doi.org/10.1115/GT2008-50834
[25] Trtchounian, Anna, Monique Williams, and Prue Talbot. "Conventional and electronic cigarettes (e-cigarettes) have different smoking characteristics." *Nicotine & Tobacco Research* 12, no. 9 (2010): 905-912. https://doi.org/10.1093/ntr/ntq114
[26] Li, Liang Chao. "CFD-DPM modeling of gas-liquid flow in a stirred vessel." In *Advanced Materials Research*, vol. 550, pp. 979-983. Trans Tech Publications Ltd, 2012. https://doi.org/10.4028/www.scientific.net/AMR.550-553.979
[27] Kleinstreuer, Clement, Zhe Zhang, and Chong S. Kim. "Combined inertial and gravitational deposition of microparticles in small model airways of a human respiratory system." *Journal of Aerosol Science* 38, no. 10 (2007): 1047-1061. https://doi.org/10.1016/j.jaerosci.2007.08.010
[28] Petit, Horacio A., Cecilia I. Paulo, Oscar A. Cabrera, and Edgardo F. Irassar. "Modelling and optimization of an inclined plane classifier using CFD-DPM and the Taguchi method." *Applied Mathematical Modelling* 77 (2020): 617-634. https://doi.org/10.1016/j.apm.2019.07.059
[29] ANSYS. *ANSYS Fluent User's Guide, Release 19.2*. ANSYS Inc., Canonsburg (2020).
[30] Morsi, S. A. J., and A. J. Alexander. "An investigation of particle trajectories in two-phase flow systems." *Journal of Fluid Mechanics* 55, no. 2 (1972): 193-208. https://doi.org/10.1017/S0022112072001806